RESEARCH ARTICLE

European Journal of
Lipid Science and Technology
www.ejlst.com

Self-Assembly of Cholesterol-Doxorubicin and TPGS into Prodrug-Based Nanoparticles with Enhanced Cellular Uptake and Lysosome-Dependent Pathway in Breast Cancer Cells

Filipe Olim, Ana Rute Neves, Mariana Vieira, Helena Tomás, and Ruilong Sheng**

Developing new easy-to-prepare functional drug delivery nanosystems with good storage stability, low hemotoxicity, as well as controllable drug delivery property, has attracted great attention in recent years. In this work, a cholesterol-based prodrug nanodelivery system is prepared by self-assembly of cholesterol-doxorubicin prodrug conjugates (Chol-Dox) and tocopherol polyethylene glycol succinate (TPGS) using thin-film hydration method. The Chol-Dox/TPGS assemblies (molar ratio 2:1, 1:1, and 1:2) are able to form nanoparticles with average hydrodynamic diameter of ≈140–214 nm, surface zeta potentials of ≈−24.2–−0.3 mV, and remarkable solution stability in 0.1 M PBS, 16 days). The Chol-Dox/TPGS assemblies show low hemotoxicity and different cytotoxicity profiles in breast cancer cells (MCF-7 and MDA-MB-231), which are largely dependent on the molar ratio of Chol-Dox and TPGS. The Chol-Dox/TPGS assemblies tend to enter into MCF-7 and MDA-MB-231 cells through non-Clathrin-mediated multiple endocytosis and lysosome-dependent uptake pathways, moreover, these nanoassemblies demonstrate lysosome-dependent intracellular localization, which is different from that of free DOX (nuclear localization). The results demonstrate that the Chol-Dox/TPGS assemblies are promising cholesterol-based prodrug nanomaterials for breast cancer chemotherapy.

***Practical Applications*: This work demonstrates a lipid prodrug-based nanotherapeutic system. Herein the Chol-Dox/TPGS nanoassemblies could serve as promising and controllable cholesterol-based prodrug nanomaterials/nano-formulations for potential breast cancer chemotherapy.**

1. Introduction

As one of the leading cancer chemotherapeutics, doxorubicin (DOX), a topoisomerase II inhibitor that intercalates with DNA, is widely employed for cancer treatment. Nevertheless, in the clinical scenario,[1] Dox has severe side effects such as high cardiotoxicity, showing a non-selective distribution, as well as multiple-drug resistance by some P-glycoprotein over-expressed tumor cells.[2–4] It has been disclosed that lipid-conjugated prodrugs could improve drug stability and present controllable drug release properties.[5,6] Some lipids (squalene,[7] palmitic acid,[8] α-linolenic acid[9] and oleic acid[10])-based DOX conjugates/complexes have been prepared, which showed improved bioavailability, reduced cytotoxicity, and enhanced drug loading/releasing efficiency in certain tumor cell lines. Thus, to overcome the shortcomings of free DOX, developing new lipid-based DOX prodrugs was regarded as a feasible approach. Moreover, for the sake of green chemistry and renewable economy, transforming biocompatible natural-based lipids[11] into molecular pharmaceutics and functional biomaterials via synthetic approaches is important for the development of sustainable biomedical engineering.

Natural steroid lipids are known as "keys of life" and play vital biological roles, including cell membrane formation, hormone metabolism, cell adhesion, and signal transduction,[12] in living organisms. Therefore, the incorporation of natural steroid-based building blocks into nanobiomaterials may bring them high biocompatibility and endow them with specific biological functions.[13–17] In earlier works, Sheng et al. prepared some bioreduction-responsive cholesterol (CHOSS) lipids[18] with high pDNA uptake/delivery efficiency and perinucleic localization effect. Moreover, they synthesized some cholesterol/lithocholate-based cationic lipids via copper(I)-catalyzed azide alkyne cycloaddition (CuAAC) "Click" approach and disclosed that the uptake/gene delivery efficiency greatly relied on the steroid structures.[19] By studying some cholesterol-based gene carrier models, they found that the physicochemical features and gene transfection properties were dependent on the cationic amino-acid headgroups rather than chemical linkages.[20] These works demonstrated that self-assembly of cholesterol- containing lipids into nanotherapeutics could lead to remarkable biological

F. Olim, Dr. A. R. Neves, Dr. M. Vieira, Prof. H. Tomás, Dr. R. Sheng
CQM – Centro de Química da Madeira, MMRG
Universidade da Madeira
Campus da Penteada, Funchal 9020-105, Portugal
E-mail: lenat@staff.uma.pt; ruilong.sheng@staff.uma.pt

The ORCID identification number(s) for the author(s) of this article can be found under https://doi.org/10.1002/ejlt.202000337

DOI: 10.1002/ejlt.202000337

European Journal of Lipid Science and Technology
www.ejlst.com

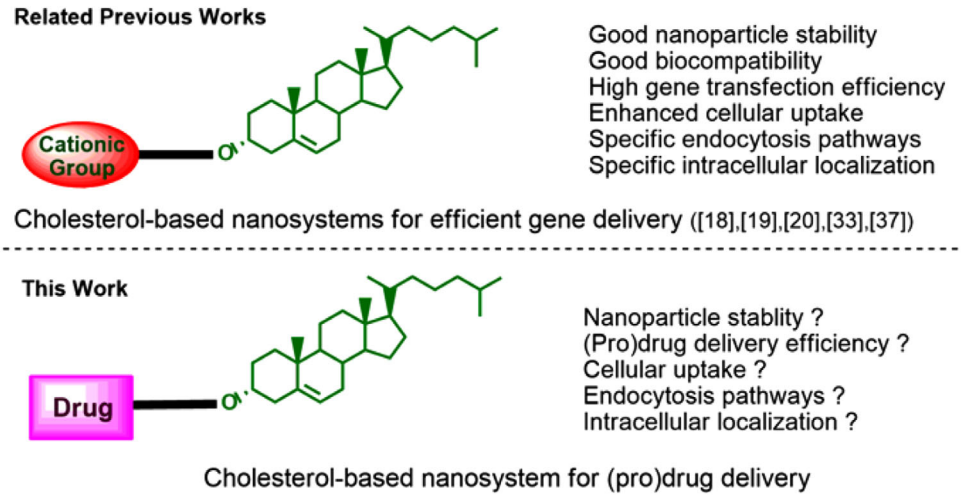

Scheme 1. From cholesterol-based gene delivery nanosystem to cholesterol-based (pro)drug delivery nanosystem.

performance (such as good serum-compatibility, low cytotoxicity, high cellular uptake, and gene transfection efficiency), which provided solid fundamental for further developing new cholesterol-based prodrug nanosystems toward drug delivery application.

Notably, many lipid-based prodrugs/conjugates are poor water-soluble, for improving their solubility, chemically/covalently linking or non-covalently assembling polyethylene glycol (PEG) chain-containing units/blocks onto the prodrug-based therapeutics has been approved as efficient methods. Moreover, the covalent/non-covalent incorporation of PEG-containing moieties could prolong the blood circulation time of nanotherapeutics, increase their accumulation and thus enhance the permeability and retention (EPR) effect.[21–23] Tocopherol polyethylene glycol succinate (TPGS), a natural-based, biocompatible, and commercially available amphiphilic lipid, has been utilized as a helper lipid in the construction of functional liposomes[24,25] or lipid nanoparticles/micelles.[26–28] It is essential to rationally incorporate TPGS with prodrugs and study the correlation between structure/chemical composition and cellular behavior. Moreover, it is very important to investigate the roles that TPGS plays in cell biological properties (e.g., cell cycle arresting, uptake/endocytosis pathways, intracellular trafficking/localization), which could provide effective feedback for further developing new prodrug/TPGS-based nanosystems with high performance and desired biofunctions.

Biologically, previous research disclosed that endocytosis pathways/mechanisms greatly affect drug/gene delivery performance.[29] In general, free cholesterol-low density lipoprotein (LDL) complexes enter into the mammalian cell through Apolipoprotein and LDL receptor-assisted uptake and Niemann-Pick C1-like transmembrane protein (NPC1)-mediated endocytosis, followed by "endosome-lysosome" intracellular transport and nuclear localization.[30] For cholesterol-containing nanobiomaterials, different endocytosis pathways were discovered. For example, Bae et al.[31] found that cholesterol-based (CHOL-E) liposomes undergo clathrin-mediated endocytosis as the dominant pathway for cellular uptake. Pozzi et al.[32] disclosed that multi-component envelope-type nanoparticle systems containing cholesterol cationic lipids (DC-Chol) were taken up by cells through the macropinocytosis pathway. Recently, Sheng et al. concluded that some steroid-(cholesterol, 2H-cholesterol, diosgenin, and tigogenin) based cationic lipids/pDNA lipoplexes mainly enter H1299 cells through caveolae and lipid-raft mediated endocytosis pathways.[33] Notably, up to date, the correlation between chemical structures and endocytosis/intracellular pathways for most of the cholesterol-based nanotherapeutic (especially nanoprodrug) systems still remains unclear and needs to be further investigated.

By the inspiration of our previous research on cholesterol-based gene delivery nanosystems, herein, we present a cholesterol-based (pro)drug delivery nanosystem (**Scheme 1**), a cholesterol-doxorubicin conjugated lipid (Chol-Dox) was synthesized and self-assembled with TPGS to construct Chol-Dox/TPGS nanoassemblies using thin-film hydration method. The physicochemical properties of Chol-Dox/TPGS assemblies were studied by dynamic light scattering (DLS) and transmission electron microscopy (TEM). The hemotoxicity of Chol-Dox/TPGS assemblies was tested by the cyanmethemoglobin assay and the cytotoxicity/inhibition efficiency was evaluated by assessing cell metabolic activity (resazurin assay method) in two breast tumor (MCF-7 and MDA-MB-231) cell lines. The cellular uptake efficiency was evaluated by flow cytometry and endocytosis pathways were studied using specific endocytosis inhibitors. Finally, the intracellular localization of the Chol-Dox/TPGS nanoassemblies was evaluated using fluorescence microscopy.

2. Results and Discussion

2.1. Synthesis and Characterization of the Chol-Dox

In DOX -based prodrugs, generally, there are two reaction sites for functional moieties conjugation: the ketone (−C=O) and amino ($-NH_2$) groups.[34] The conjugates should be degradable/cleavable under the intracellular acidic environment[35] (e.g., inside lysosome) and thus result in the release of DOX. Herein, by one-step coupling of cholesteryl chloroformate with 1° amine group on the sugar ring of DOX, followed by flash

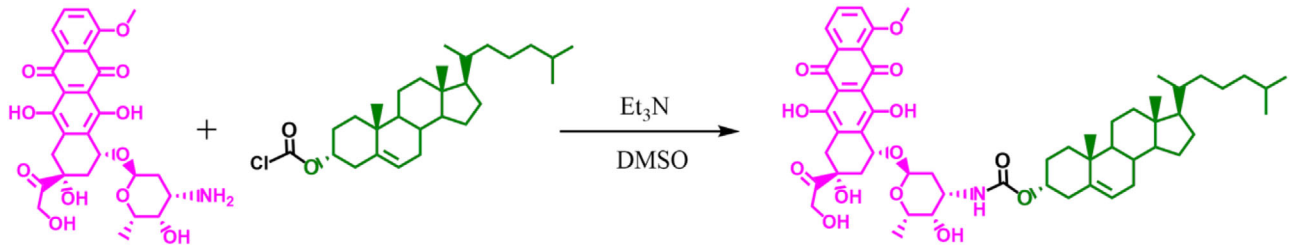

Scheme 2. Synthesis and molecular structure of the cholesterol-doxorubicin lipid conjugate (Chol-Dox).

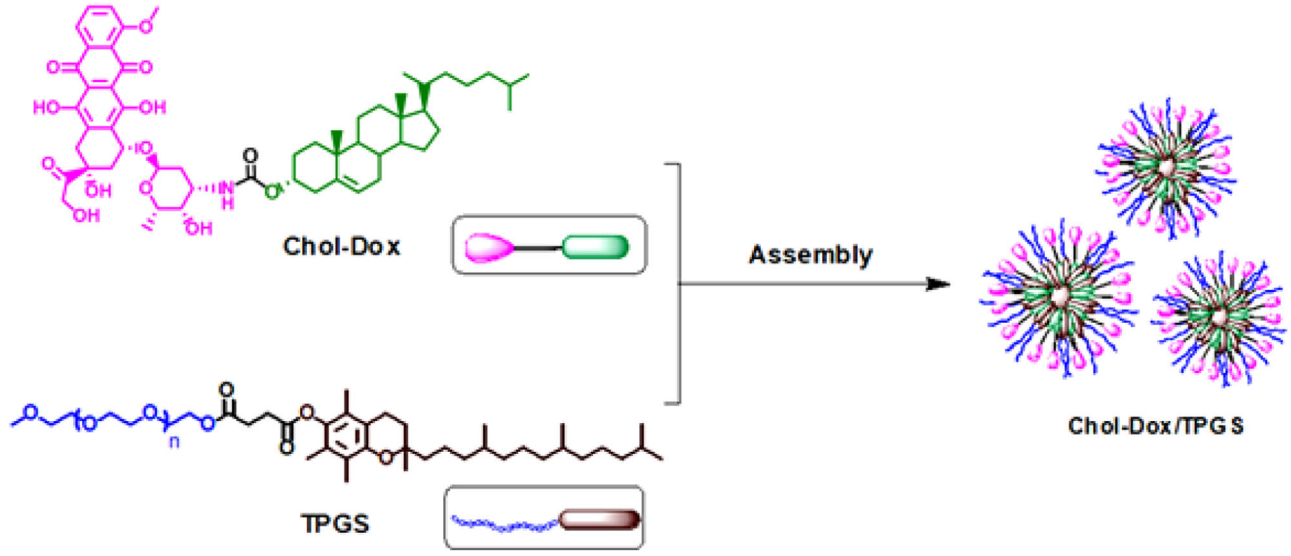

Scheme 3. Preparation of Chol-Dox/TPGS nanoassemblies by incorporation of TPGS with Chol-Dox in aqueous solution.

column chromatography purification, we prepared a Chol-Dox through a facile and modular synthetic method (**Scheme 2**), with the isolation yield of 83%. The molecular structural characterization by NMR and MS was described in detail in the experimental part, and the ^{1}H, ^{13}C NMR, and ESI-MS spectra of Chol-Dox are shown in Figure S1, Supporting Information. In the ^{1}H NMR spectrum, the peaks at 13.97 and 13.21 ppm are identified as the phenol proton signals, and peaks at 7.41, 7.34, and 7.28 ppm are signals of the aromatic protons of DOX. An obvious double bond proton signal of cholesterol could be seen at ≈5.2–5.3 ppm. The multiple signals ≈2.23–0.74 ppm belong to the hydrophobic cholesterol[18,19,33,36,37] skeletons. The results indicate that the new Chol-Dox was successfully prepared via a facile, mild, and efficient synthetic approach.

2.2. Preparation of Chol-Dox/TPGS Assemblies and Their Physico-Chemical Properties (Hydrodynamic Diameter and Zeta Potential)

The as-synthesized Chol-Dox systems are highly hydrophobic and poor-water soluble. To prepare a nano-formulation with good water solubility and achieve enhanced-drug delivery properties, Chol-Dox was self-assembled with TPGS at predetermined molar ratios (1:2, 1:1, 2:1, v:v) by lipid thin-film hydration method (**Scheme 3**).[36,38] The Chol-Dox/TPGS assemblies were obtained as transparent red-colored solutions.

Table 1. Hydrodynamic diameter (z-average, nm), polydispersity index (PDI), and zeta potential of the Chol-Dox/TPGS nanoassemblies.

Samples	Z-average [nm]	Polydispersity [PDI]	Surface zeta potential [mV]
Chol-Dox	-	-	-
Chol-Dox/TPGS 2:1	214 ± 6	0.353	−24.2 ± 0.4
Chol-Dox/TPGS 1:1	140 ± 4	0.347	−7.3 ± 0.7
Chol-Dox/TPGS 1:2	141 ± 3	0.318	−−0.3 ± 0.1

It has been disclosed that the therapeutic efficiency of drug/gene nanocarriers greatly relies on their physicochemical properties (such as particle size, zeta potential, morphology, stability, and so on).[39] In our exploration of solution self-assembly conditions, we found that the particle size of Chol-Dox/TPGS assemblies largely depends on the Chol-Dox/TPGS ratio. At high Chol-Dox/TPGS ratios of 2:1, small nanoparticles were difficult to be formed, due to the high hydrophobicity of Chol-Dox; at lower Chol-Dox/TPGS ratios of 1:1 and 1:2, smaller nanoparticles (around 140 nm, **Table 1**) were formed, since the high concentration of TPGS can serve as a hydrophilic auxiliary agent to increase the solubility of the poorly-water soluble Chol-Dox. Moreover, the ultrasonication time is also an essential factor. A prolonged ultrasonication time will lead to better dispersion (polydispersity (PDI) < 0.25) and smaller average particle sizes

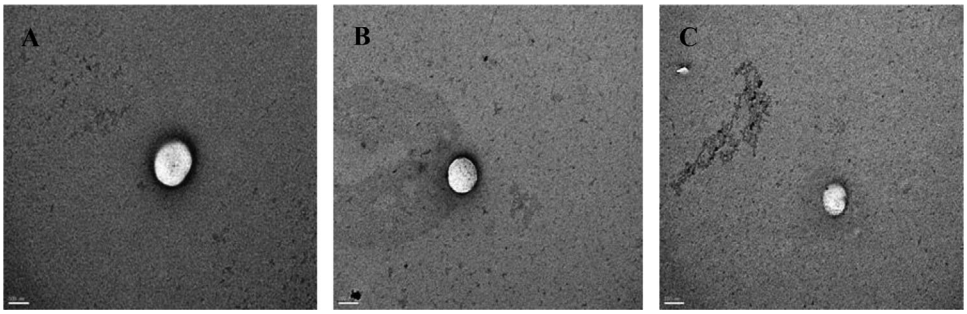

Figure 1. TEM images of the Chol-Dox/TPGS nanoassemblies. A) Chol-Dox/TPGS 2:1; B) Chol-Dox/TPGS 1:1; C) Chol-Dox/TPGS 1:2;scale bar: 100 nm. It could be seen that Chol-Dox/TPGS assemblies are near-spherical solid nanoparticles.

(<220 nm). Likewise, in previous work, Sheng et al. reported that the co-assembly of the diosgenin-based cationic lipid with the hydrophilic DOPE helper lipid could lead to the formation of Dios-Arg/DOPE nanoparticles with small hydrodynamic size, which brings about high pDNA/siRNA binding affinity and efficient gene transportation efficiency.[36] The present results indicated that the particle size of the Chol-Dox/TPGS assemblies could be tuned by choosing certain Chol-Dox/TPGS molar ratio and optimizing the ultrasonication time.

It has been disclosed that drug delivery and cellular internalization/trafficking mechanisms of nanobiomaterials largely rely on their hydrodynamic particle size, surface charge, and shape/morphology,[33,40] these physicochemical properties were dependent on the molecular factors including: structure/geometry, hydrophobicity/hydrophilicity, and component ratios.[41] Herein, the hydrodynamic diameter, PDI, and surface charge of Chol-Dox/TPGS assemblies were measured. As shown in Table 1, the Chol-Dox and TPGS are able to form nanoaggregates in aqueous solution. The average hydrodynamic diameter of Chol-Dox/TPGS assemblies (2:1, 1:1, and 1:2) is ≈140–214 nm with moderate size distributions (PDI ≈0.318–0.353, original profiles were shown in Figure S2, Supporting Information. The decrease of Chol-Dox/TPGS ratio (increase of assemblies' hydrophilicity) will lead to smaller particle size.[39,40] Delightfully, the obtained particle size is suitable for efficient intracellular uptake and may be beneficial for intracellular drug delivery and nuclear localization.[18,36,42] Meanwhile, different surface charges (zeta potentials) of the Chol-Dox/TPGS assemblies were observed. Chol-Dox/TPGS assemblies (2:1 and 1:1) demonstrated relatively higher negative surface charges of −24.2 and −7.3 mV, whilst Chol-Dox/TPGS assemblies (1:2) showed less negative surface charges −0.3 mV, which may due to the charge shielding ("stealth") effect of the linear PEG-1000 chain attached to TPGS. The results indicated that the surface charge could be tuned/controlled by choosing certain Chol-Dox and TPGS amounts/ratios. Moreover, the different surface charge values among Chol-Dox/TPGS assemblies (2:1, 1:1, and 1:2) suggested that they may possess different cellular uptake capability, drug delivery efficiency, as well as intracellular behavior.[20]

Morphology of the Chol-Dox/TPGS nanoassemblies was investigated by TEM. In **Figure 1**, the Chol-Dox/TPGS assemblies were observed as near-spherical solid nanoparticles.[18] Compared to the double chain-bearing helper lipids such as dioleoylphosphatidylethanolamine (DOPE) and 1,2-dioleoyl-3-trimethylammonium propane (DOTAP), single chain-bearing TPGS tend to form solid nanoparticles instead of bilayer liposomes with lamellar phase structure. Similarly, Feng et al disclosed that a vitamin E TPGS-cisplatin prodrug could be assembled into solid nanoparticles.[24] Moreover, it could be noticed that the trend of particle size for Chol-Dox/TPGS assemblies measured by TEM was in good accordance with the DLS results.

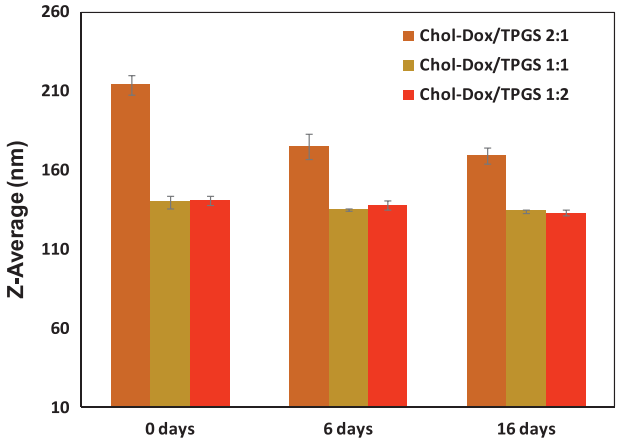

Figure 2. In solution stability of the Chol-Dox/TPGS assemblies at various molar ratios (2:1 1:1 and 1:2).

2.3. In-Solution Stability of the Chol-Dox/TPGS Assemblies

For practical applications, the drug-loaded lipid nanoparticles/assemblies should be stable enough for storage and the possible dissociation under storage conditions should be avoided to maintain bioavailability. Misra et al. reported that the solution storage stability of a nano-formulation could affect their gene delivery properties.[43] Herein, we examined the solution stability of Chol-Dox/TPGS assemblies in PBS (1×) solution by measuring the hydrodynamic diameter at pre-determined times (0, 6, 16 days) by DLS. As shown in **Figure 2**, the less hydrophobic Chol-Dox/TPGS (1:2 and 1:1) assemblies showed negligible particle size change and the more hydrophobic Chol-Dox/TPGS (2:1) assemblies showed a slight decrease of size after 16 days of incubation. The high stability may be due to the strong hydrophobic interactions among the cholesterol and tocopherol hydrophobes.[44] Notably, the stability sequence of Chol-Dox/TPGS 1:2 ≈ 1:1 > 2:1

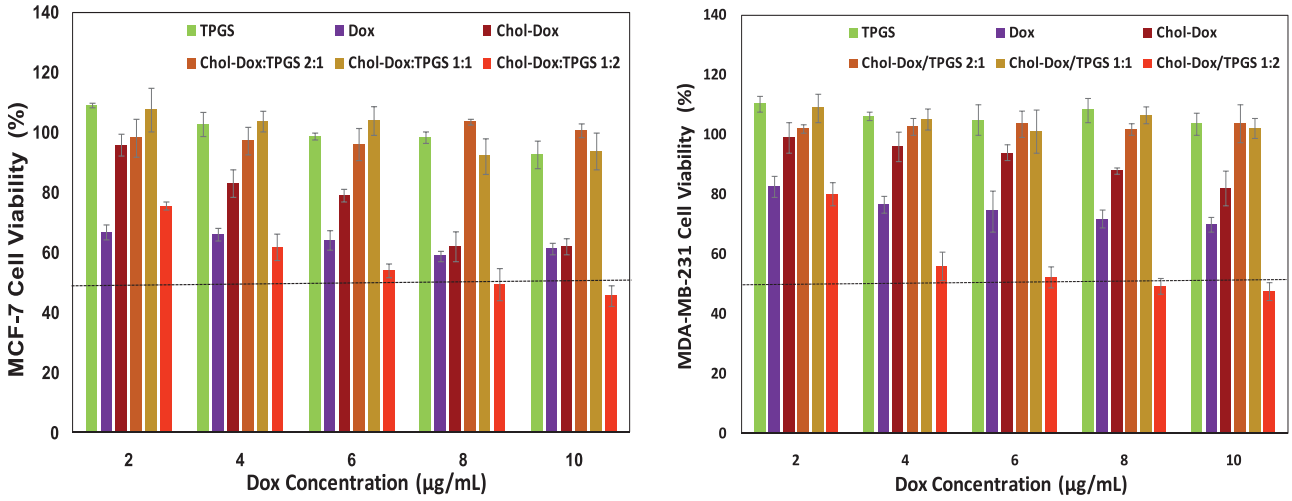

Figure 3. Apparent cytotoxicity of the Chol-Dox/TPGS assemblies in a) MCF-7 cells and b) MDA-MB-231 cells; TPGS, free Dox, and Chol-Dox were used as controls; experiments were made at equivalent doxorubicin concentrations (from 0 to 10 μg mL^{-1}).

showed that the combination of TPGS helper lipid[45] with the hydrophobic Chol-Dox prodrug could enhance nanoformulation's stability, which may benefit their drug delivery efficiency.

2.4. Cytotoxicity of the Chol-Dox/TPGS Assemblies

The in vitro cytotoxicity of the Chol-Dox/TPGS assemblies was evaluated in two breast cancer cell lines (MCF-7 and MDA-MB-231) using a metabolic activity assay (the resazurin reduction assay) with free TPGS and free DOX as controls. As shown in **Figure 3**a,b, the TPGS helper lipid showed negligible cytotoxicity in MCF-7 and MDA-MB-231 cell lines (viability > 93.0%), whereas free Dox demonstrated high cytotoxicity (viability ≈63.0–68.2% in MCF-7 and ≈75.2–82.5% in MDA-MB-231), which possibly due to its topoisomerase II inhibition and DNA intercalation effects.[46] The Chol-Dox conjugate showed less cytotoxicity than free Dox (≈92.7–98.5%in MCF-7 and ≈78.1–115.4%in MDA-MB-231) due to the covalent conjugation on the amine group.[9] Notably, the Chol-Dox/TPGS assemblies have very different cytotoxicity behavior within the tested Dox concentration range (from 0 to 10 μg mL^{-1}). Chol-Dox/TPGS assemblies of 2:1 and 1:1 showed low cytotoxicity (viability ≈105.6–96.5% in MCF-7 and ≈106.7–114.7%in MDA-MB-231). Dramatically, the Chol-Dox/TPGS assemblies (1:2) showed remarkable cytotoxicity (viability ≈42.5–75.6% in MCF-7 and ≈47.7–79.1% in MDA-MB-231) and their IC_{50} values (≈8.0 μg mL^{-1} for both MCF-7 and MDA-MB-231 cell lines) were lower than that of free Dox (IC_{50} > 10.0 μg mL^{-1}), indicating the TPGS ratio greatly affects the apparent cytotoxicity of Chol-Dox/TPGS assemblies. These results suggested that cytotoxicity can be controlled by incorporating TPGS into Chol-Dox prodrug for the construction of Chol-Dox/TPGS assemblies, while the enhanced cytotoxicity mechanism is not clear yet. Likewise, in previous work, Sheng et al. have revealed that the apparent cytotoxicity of Dios-Arg/DOPE nanoparticles greatly relied on the ratio of hydrophilic DOPE helper lipid.[36]

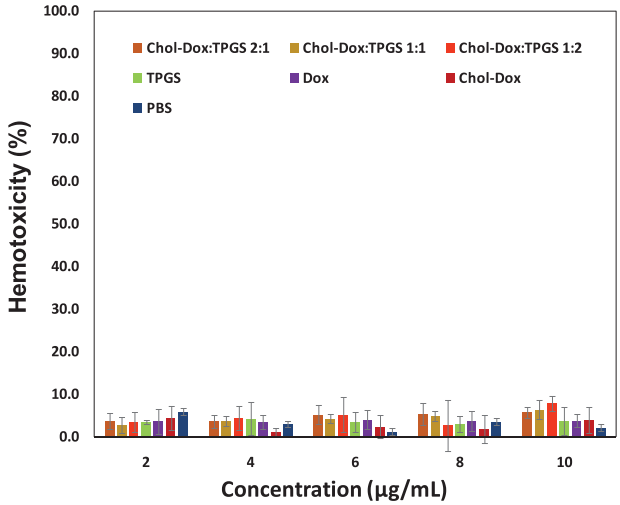

Figure 4. Hemotoxicity (% of hemolysis) of Chol-Dox/TPGS assemblies in red blood cells; TPGS, free Dox, and Chol-Dox were used as controls; experiments were made at equivalent doxorubicin concentrations (from 0 to 10 μg mL^{-1}). It showed that Chol-Dox/TPGS assemblies have low hemotoxicity.

2.5. Hemotoxicity of the Chol-Dox/TPGS Assemblies

Besides cytotoxicity, hemotoxicity is an essential parameter for the evaluation of biocompatibility of nanomaterials to be administered in blood circulation systems, which will inevitably have contact with blood cells, especially red blood cells, and possibly induce hemotoxicity and diminish their therapeutic efficacy. Herein the hemotoxicity of Chol-Dox/TPGS assemblies in human red blood cells was measured by hemoglobin assay. As shown in **Figure 4**, the Chol-Dox/TPGS assemblies, TPGS, Chol-Dox, and free Dox showed low hemotoxicity (<9.8%), which may be due to the shielding effect of PEG chains and

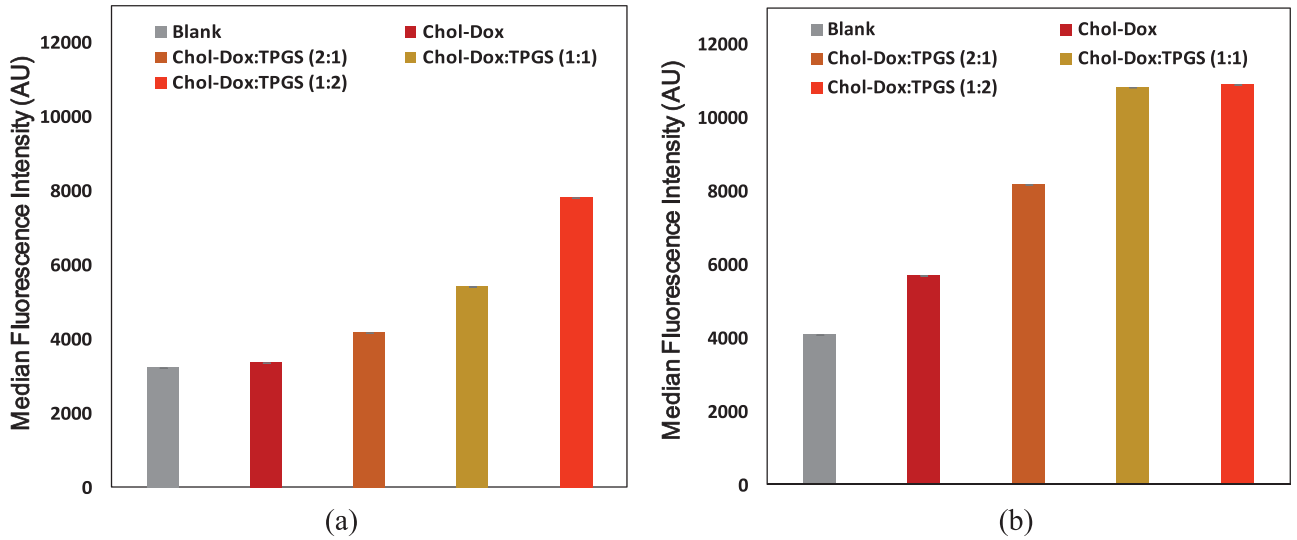

Figure 5. Intracellular uptake of Chol-Dox/TPGS nanoassemblies in a) MCF-7 and b) MDA-MB-231 cell lines by flow cytometry using Chol-Dox as the control, it indicated that the intracellular uptake increased with the increasing of TPGS ratio.

negatively-charged surface that decreased the interactions of Chol-Dox/TPGS assemblies with the blood cell membranes. The results indicated that Chol-Dox/TPGS assemblies could be employed as low hemotoxic and biocompatible nanoformulations for potential in vivo drug administration.

2.6. Cellular Uptake of Chol-Dox/TPGS Assemblies in MCF-7 and MDA-MB-231 Cells

Cellular uptake capability is an essential factor that determines the transport/delivery efficiency of drug/gene therapeutics.[47] Herein, by using the red-fluorescent emission of Chol-Dox/TPGS assemblies, we quantitatively analyzed the cell uptake efficiency by flow cytometry, with Chol-Dox and free Dox used as controls (the original flow cytometry profiles are shown in Figure S3, Supporting Information). As shown in **Figure 5**a,b, the Chol-Dox conjugates have relatively lower cellular uptake capability, which might be due to their poor water solubility and negative charge on the deprotonated phenol groups of DOX. Compared to Chol-Dox (uptake capability set as 100%), much higher cellular uptake capability were observed for the Chol-Dox/TPGS (2:1) assemblies (125.5% in MCF-7 and 144.2% in MDA-MB-231 cells) and Chol-Dox/TPGS (1:1) assemblies (162.2% in MCF-7 and 190.1% in MDA-MB-231 cells). The Chol-Dox/TPGS (1:2) assemblies showed the highest cell uptake capability (234.3% in MCF-7 and 192.5% in MDA-MB-231), indicating that the incorporation of TPGS could largely increase the uptake process. As aforementioned, the incorporation of TPGS is associated to a higher PEG-shielding effect and increased surface zeta potential (from −24.2 to −0.3 mV), thus leading to an enhancement of cellular uptake. Likewise, in an earlier work, Sheng et al. demonstrated that the incorporation of DOPE helper lipids into Diosarg cationic lipids could increase the surface zeta potential and related cellular uptake.[36] It can be deduced that the highest cellular uptake capability of Chol-Dox/TPGS (1:2) assemblies lead to the highest DOX delivery efficiency and thus cause remarkable inhibition effect on the breast tumor cells.[47] Overall, the results showed that the cellular uptake efficiency could be adjusted/tuned by incorporating certain lipid amphiphiles with the DOX prodrug.

2.7. Endocytosis Pathway Analysis of the Chol-Dox/TPGS Assemblies

Nanomaterials were reported to enter mammalian cells through several endocytosis pathways including: clathrin-mediated endocytosis (inhibitor: Chlorpromazine), caveolae/lipid-raft-mediated endocytosis (inhibitor: Filipin III), macropinocytosis (inhibitor: cytochalasin D), microtubule-assisted phagocytosis (inhibitor: Nocodazole), and lysosome-dependent pathway (inhibitor: Nigericin). When nanomaterials are used as drug carriers, these different pathways have been shown to be related with drug delivery efficiency.[29,48,49] To study the endocytosis mechanisms of Chol-Dox/TPGS assemblies, their cellular uptake was analyzed by flow cytometry in the presence of various endocytosis-specific inhibitors (the uptake efficiency of Chol-Dox/TPGS assemblies without endocytosis inhibitors was set as 100%). As shown in **Figure 6**a, in MCF-7 cells (estrogen receptor + (ER+), progesterone receptor + (PR+), human epithelial growth factor receptor–(HER2-)),[50] Chol-Dox prodrug enters cells mainly through macropinocytosis, which is different from free Dox (passive diffusion[4]). Notably, Chol-Dox/TPGS assemblies undergo multiple endocytosis pathways (mostly microtubule-dependent phagocytosis) and lysosome-dependent intracellular pathway, but non-Clathrin-mediated and non-Caveolae/lipid-raft-mediated. The endocytosis feature of Chol-Dox/TPGS may be attributed to the combination effect of hydrophilic TPGS, cholesterol-based structure, and lysosome-degradable carbamate ester. On the other hand, as shown in Figure 6b, different endocytosis pathways were observed in MDA-MB-231 cells (ER-, PR-,[50] HER2-). The Chol-Dox prodrug enters into MDA-MB-231 cells through multiple endocytosis

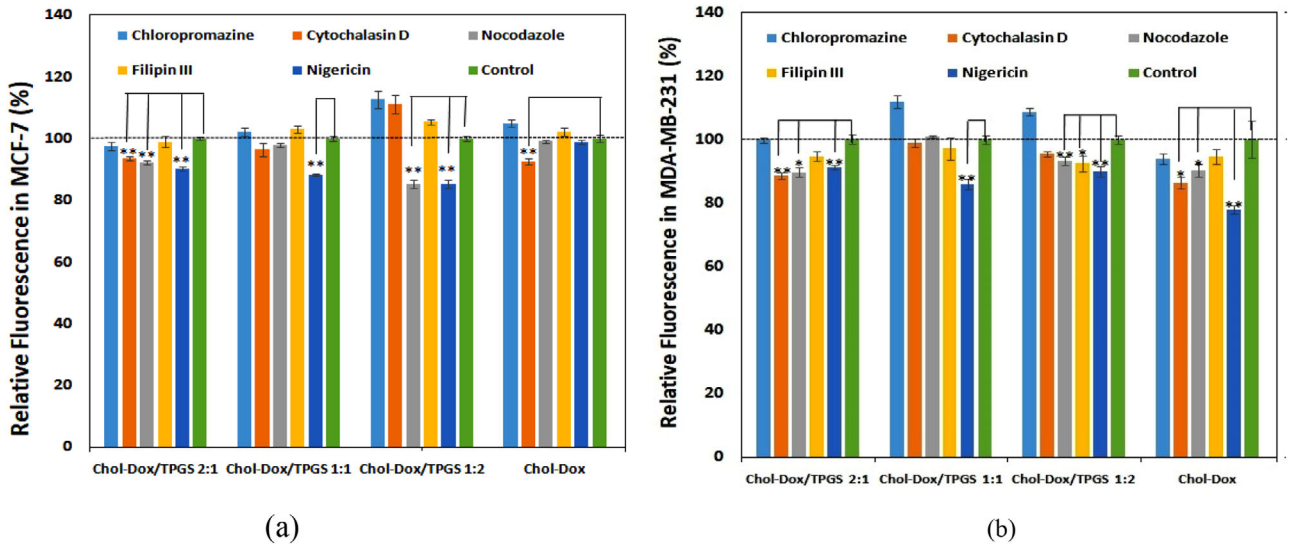

Figure 6. Endocytosis pathway analysis of the Chol-Dox/TPGS assemblies in a) MCF-7 and b) MDA-MB-231 cells by measuring the relative uptake efficiency with endocytosis-specific inhibitors (*$p < 0.05$, **$p < 0.001$).

pathways; the lysosome-dependent property may be attributed to its cholesterol-based structure and lysosome-degradable carbamate ester as well. For Chol-Dox/TPGS assemblies, they tend to enter MDA-MB-231 cells through multiple pathways too (mainly macropinocytosis and microtubule-dependent phagocytosis), but not through Clathrin-mediated pathway, which may be due to the strong hydrophilicity of TPGS. Chol-Dox/TPGS assemblies also have a lysosome-dependent intracellular pathway. The results showed that, to some extent, introducing TPGS could lead to non-Clathrin-mediated multiple endocytosis pathways. Likewise, some PLA-PEG-containing nanoparticles enter the in bEnd.3 cell through a macropinocytosis pathway instead of Clathrin-mediated pathway.[51] Notably, the strong lysosome- dependent feature of Chol-Dox/TPGS may be beneficial for the lysosomal enzyme-induced Dox release from the nanoassemblies.[52] Moreover, the different endocytosis profiles of MCF-7 and MDA-MB-231 cells suggested that cell surface receptor (ER/PR) phenotypes may play important roles in the determination of uptake efficiency and endocytosis pathways.

2.8. Intracellular Localization of the Chol-Dox/TPGS Assemblies

To get more insight of the cellular fate, the intracellular localization of the Chol-Dox/TPGS assemblies in MCF-7 (**Figure 7**) and MDA-MB-231 cells (Figure S4, Supporting Information) was observed under fluorescence microscope, with Chol-Dox and free Dox as the control. The cell nuclei and lysosomes were separately labeled/stained with the fluorescent dyes Hoechst 33258 (blue fluorescent) and Lysotracker (green), respectively. As shown in Figure 7, in MCF-7 cells, after incubation with free Dox, strong red fluorescent spots were found within the entire cells; they were able to co-localize with the Hoechst 33258-stained nucleus and also co-localize with the lysotracker-stained lysosome, due to the fast diffusion of water-soluble small molecule DOX. Chol-Dox, the lipid conjugate of DOX, was mostly located outside the cell and some of them were shown to adhere to the cell membrane, which may be due to the presence of cholesterol that acted as a docking moiety. Meanwhile, in the case of Chol-Dox/TPGS nanoassemblies, different intracellular localization profiles were observed. For the cells incubated with Chol-Dox/TPGS 2:1, red fluorescent spots were observed dispersed around/outside the cells and a comparatively weaker red fluorescence could be observed inside the cells, indicating their low cellular uptake capability. For the cells incubated with Chol-Dox/TPGS 1:1 and 1:2, stronger red fluorescence inside the cells could be observed. Notably, lysosome co-localization effects[33] of these assemblies were observed, indicating that the introduction of TPGS could remarkably enhance the intracellular uptake of Chol-Dox and lead to lysosome localization. Similar intracellular localization of the Chol-Dox/TPGS nanoassemblies was also observed in MDA-MB-231 cells (Figure S4, Supporting Information), indicating that intracellular trafficking of the nanoassemblies was not cell type-dependent.

Accordingly, we proposed an intracellular trafficking mechanism of Chol-Dox/TPGS assemblies as follows: first, the Chol-Dox/TPGS assemblies entered cancer cells through multi-pathway (macropinocytosis/phagocytosis)-mediated endocytosis; second, the assemblies underwent endosome-lysosome internalization pathway and then localized inside lysosome; finally, the assemblies were dissociated in lysosome and followed with esterase-assisted hydrolysis of the prodrug Chol-Dox. The results indicated that molecular/structural factors imposed by Chol-Dox/TPGS (prodrug/helper lipid) ratios remarkably affected the cellular uptake and localization of the nanoassemblies, which allows a possible way to control their biological behavior.

3. Conclusions

In this work, we developed a cholesterol-based (pro)drug delivery nanosystem by self-assembly of Cholesterol-Doxorubicin prodrug and TPGS using thin-film hydration method. The

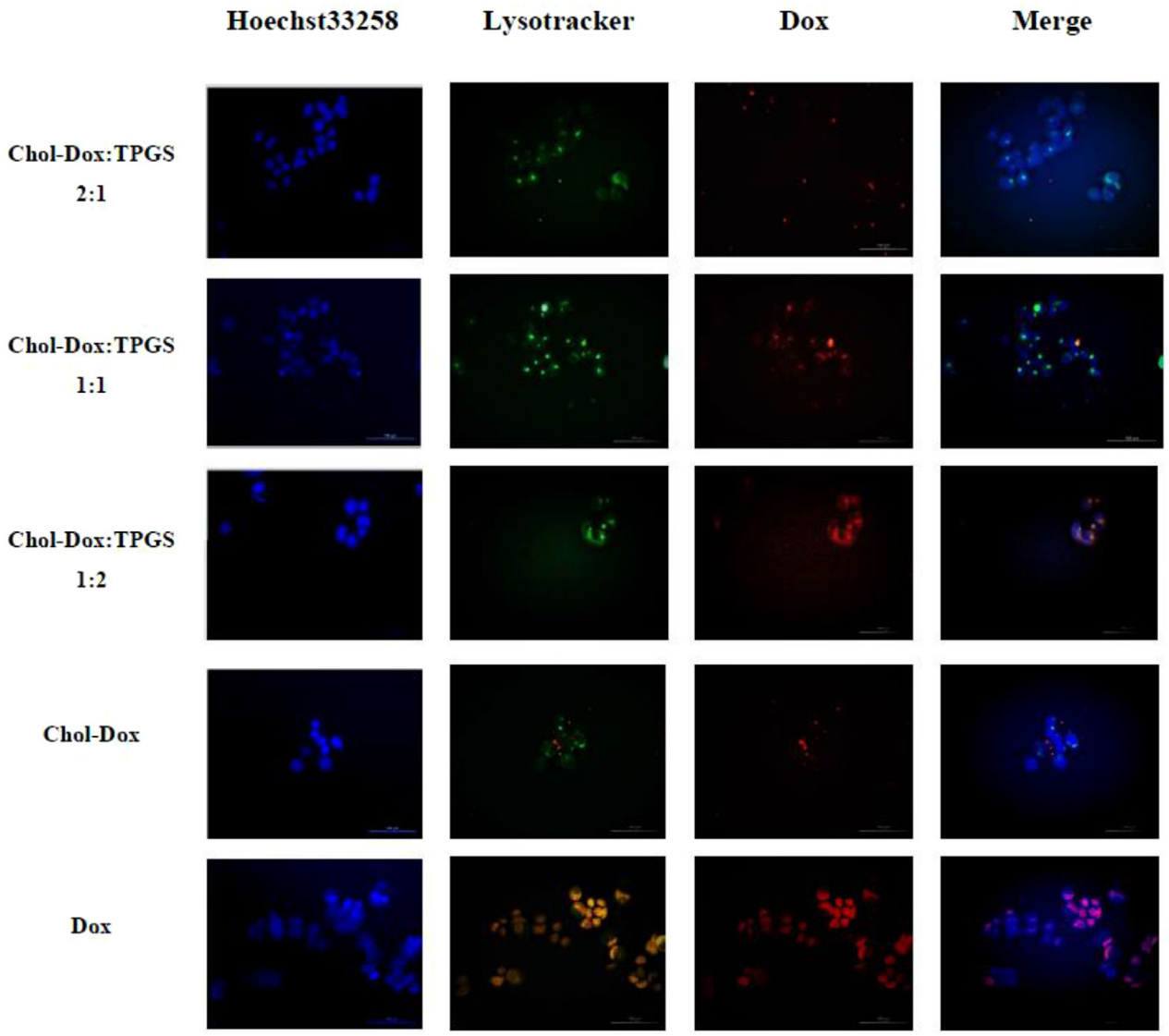

Figure 7. Intracellular localization of the Chol-Dox/TPGS assemblies in MCF-7 cells, Chol-Dox, and free Dox were used as controls (scale bar: 100 μm). It showed that, compared to free Dox and Chol-Dox, Chol-Dox/TPGS assemblies have different intracellular localization effects, moreover, introduction of TPGS could lead to efficient lysosome localization.

Chol-Dox/TPGS assemblies (molar ratio 2:1, 1:1, and 1:2) were able to form nanoparticles with average hydrodynamic particle diameter of ≈140–214 nm, surface zeta potential of ≈−24.2–−0.3 mV, and remarkable solution stability in 0.1 M PBS. The Chol-Dox/TPGS assemblies showed low hemotoxicity and different cytotoxicity profiles in distinct types of breast cancer cells (MCF-7 and MDA-MB-231), which was largely dependent on the molar ratio of Chol-Dox and TPGS. Moreover, the Chol-Dox/TPGS assemblies seem to enter MCF-7 and MDA-MB-231 cells through non-Clathrin-mediated endocytosis and lysosome-dependent pathways. The endocytosis pathways seem to depend, to some extent, on the type of breast cancer cells. Moreover, the Chol-Dox/TPGS assemblies showed lysosome-dependent intracellular localization, different from that of free DOX. The results demonstrated that the Chol-Dox/TPGS assemblies could be employed for the inhibition of breast cancer cell proliferation, making them potential candidates for breast cancer chemotherapy. Notably, this work established sustainable (pro)drug delivery nanosystems from natural lipid-based prodrug conjugates via easy-to-manipulate synthesis and self-assembly approaches. It can be anticipated that, in future research, stimuli-responsive (e.g., disulfide[18] and Schiff-base[53]) linkers and targeting-ligands (e.g., glucosamine[54] and cell penetrating peptides[55]) could be further introduced to construct natural lipid-based "smart" nano-therapeutics toward nanomedicine applications.

4. Experimental Section

Materials: Cholesterol chloroformate (98.0%) was purchased from Sigma Aldrich and used as received. DOX hydrochloride (99.0%) was purchased from Haizheng Pharma. Co. Ltd, China, and used as received.

Tocopheryl polyethylene glycol 1000 succinate TPGS (98.0%) was purchased from Aladdin, China, and used as received. Other reagents and solvents were analytical grade and also used as received.

Resazurin sodium salt (75.0% of dye content) was bought from Sigma Aldrich and dissolved in PBS (phosphate buffer solution, Sigma Aldrich) to prepare the solution (0.1 mg mL^{-1}) for the cytotoxicity assays. RPMI-1640 culture medium and 10% fetal bovine serum (FBS) were purchased from Gibco-Thermo Fisher. The antibiotic-antimycotic solution was bought from Sigma Aldrich. 96-well, 24-well micro plates were purchased from VWR, International, LLC. Human blood samples from healthy donors were obtained from Hospital Nélio Mendonça, Funchal, Portugal (no blood was withdrawn specifically for the studies; only the blood remaining from clinical interventions was used). Human breast cancer MCF-7 and MDA-MB-231 cell lines were purchased from DSMZ (Braunschweig, Germany). The endocytosis specific inhibitors: chlorpromazine hydrochloride (98.0%), cytochalasin D (98.0%), nigericin sodium salt (98.0%), nocodazole (99.0%), and filipin III (85.0%) were purchased from Sigma Aldrich. Lysotracker green DND-26 (lysosome staining agent) was received from Invitrogen-Thermo Fisher and Hoechst 33258 (nuclear staining agent) from Sigma Aldrich. In addition, all the other reagents and chemicals were of analytical grade and were utilized as received.

Synthesis Procedure of Chol-Dox: DOX hydrochloride (58 mg, 1 mmol) was placed in a two-necked round bottom flask with a solution of 1 mL dimethylsulfoxide (DMSO)/0.5 mL methanol/0.5 mL triethylamine. Then cholesteryl chloroformate (60 mg, 1.5 mmol) in a solution of 1 mL DMSO/1 mL tetrahydrofuran was added and the mixture was stirred for 24 h under room temperature. After the reaction was completed, the mixture was concentrated, poured into 100 mL saturated NaCl solution, and extracted with 100 mL CH_2Cl_2. The water layer was discarded, and the organic layer was separated and washed with saturated NaCl solution and dried over anhydrous Na_2SO_4. The residue was purified by silica gel column chromatography using $CHCl_3$/Methanol (10/1, v/v) as eluent to give the Chol-Dox as a red solid compound (78.4 mg, yield: 83%). The molecular structure of Chol-Dox was characterized by NMR and MS (the original profiles are shown in Figure S1, Supporting Information).

NMR, IR, and Mass Spectrometry Measurements: ^{1}H (400 MHz) and ^{13}C (100 MHz) NMR spectra were recorded on an Avance II+ 400 spectrometer (Bruker, Wissembourg, France) at 299 K (probe temperature). The chemical shifts were reported in parts per million (ppm). Infrared (IR) spectra were recorded on an Avatar 360 FTIR (Nicolet, ThermoScientific, Waltham, MA, USA) in KBr pellets; only significant bands were mentioned in the text. The mass spectra (ESI-MS) were recorded with a Micromass LCT mass spectrometer (Waters, Milford, MA, USA).

Co-Assembly of the Chol-Dox and TPGS in Aqueous Solution: Chol-Dox and TPGS were individually dissolved into a solution of acetone/chloroform (90/10) to prepare stock solutions with the same concentration (1×10^{-3} M). Then a predetermined amount of Chol-Dox and TPGS containing solutions were mixed together in 10 mL vials to obtain volume ratios of 1:2, 1:1, 2:1, followed by the removal of organic solvents under nitrogen atmosphere to prepare lipid thin-films. Afterward, PBS (1×) solution was added into the vials with gentle shaking, the vials were put in an ultrasonic water bath and then treated with ultrasound for 5 h. Finally, the solution was filtrated through a membrane (0.22 µM) to prepare the Chol-Dox/TPGS assemblies (1:2, 1:1, 2:1).

Hydrodynamic Diameter and Zeta Potential of the Chol-Dox/TPGS Assemblies: Average particle size and zeta potential of the Chol-Dox/TPGS assemblies were analyzed in a Malvern Zetasizer Nano ZS90 (UK) at room temperature by DLS and electrophoretic light scattering techniques, respectively. The as-prepared Chol-Dox/TPGS assembly solutions (50 µL) were added into 1 mL pure water, and then laser light at $\lambda = 633$ nm was employed at a fixed scattering angle of 90° for nanoparticle size analyses.

For investigating the stability of Chol-Dox/TPGS assemblies in aqueous solution, the as-prepared assemblies were incubated with 0.1 M PBS buffer solution for predetermined periods (0, 6, 16 days at room temperature), and then the average particle size was analyzed by DLS.

Morphology of the Chol-Dox/TPGS Assemblies by TEM: TEM was used to study the morphology of Chol-Dox/TPGS assemblies (1:2, 1:1, 2:1) at room temperature. For TEM analysis, 10 µL of the as-prepared Chol-Dox/TPGS solution samples were mounted on Formvar/carbon film-coated mesh nickel grids (Electron Microscopy Sciences, Hatfield, PA, USA) and left standing for 2 min. The liquid in excess was removed with filter paper and the grids stained with 10 µL of uranyl acetate for 10 s. Visualization was carried out on a JEOL JEM 1400 TEM with an acceleration voltage of 120 kV (Tokyo, Japan). Images were digitally recorded using a CCD digital camera Orious 1100W Tokyo, Japan.

Cytotoxicity of the Chol-Dox/TPGS Assemblies: Breast tumor cell proliferation inhibition caused by Chol-Dox/TPGS nanoassemblies was examined using MCF-7 and MDA-MB-231 cell lines by resazurin reduction assay. Chol-Dox, TPGS, and free DOX were used as controls. After cell seeding in 96-well plates (5×10^3 cells/well) and 24 h incubation, the medium was removed and replaced by 200 µL fresh RPMI-1640 medium supplemented with 10% FBS and 1% antibiotic-antimycotic solution. Then the nanoassembly samples (Chol-Dox/TPGS 2:1, 1:1, 1:2) and control solution (in PBS) were added into the MCF-7 and MDA-MB-231 cells to get final DOX concentrations of ≈0–10 µg mL^{-1}. The cultures were then further incubated at 37 °C under 5% CO_2 for 24 h. For the analysis, 200 µL of fresh supplemented RPMI-1640 medium with 0.01 mg mL^{-1} resazurin was added to each well and incubated for another 4 h. The relative resorufin fluorescence was measured ($\lambda_{ex} = 530$ nm, $\lambda_{em} = 590$ nm) using a Victor^3 1420, PerkinElmer microplate reader. Results were presented as relative fluorescence units (RFU) and 4 replicates were done for each sample ($n = 4$). Cell viability was normalized to that of cells treated with only PBS buffer as the indicator of 100% cell viability. Relative cell viability was calculated as follows.

$$\text{Cell viability (\%)} = \text{RFU}_{(\text{Sample})} \times 100\%/\text{RFU}_{(\text{Control})} \quad (1)$$

Hemotoxicity of the Chol-Dox/TPGS Assemblies by Hemoglobin Assay: The human blood samples were diluted to prepare a 10% blood solution in 1 × PBS (Mg^{2+}/Ca^{2+} free). For the hemotoxicity assay, blood solutions (10 µL) were taken into microcentrifuge tubes, and then predetermined amounts of samples (Chol-Dox/TPGS assemblies) were added (in 70 µL) and incubated at 37 °C for 3 h. Hemotoxicity effect of the TPGS, Chol-Dox, and free Dox was also analyzed, using distilled water as the positive control and 1 × PBS (70 µL) as the negative control. Then the tubes were centrifuged at 3800 rpm for 5 min. 40 µL of each supernatant were transferred into 96-well plates and 160 µL of cyanmethemoglobin reagent was added. This reagent was prepared with 50 mg potassium ferricyanide, 12.5 mg potassium cyanide, 35 mg potassium dihydrogen phosphate, and 250 µL Triton-X in 250 mL of distilled water (in an amber bottle), and its pH was adjusted to 7.4. The total concentration of hemoglobin in the original blood was determined using a 250-fold dilution of blood in cyanmethemoglobin reagent, followed by filtration with a low-binding, low-release membrane filter (0.22 µm PVDF filter, Millipore). The absorbance at 540 nm was measured in the microplate reader (Victor^3 1420, PerkinElmer).

Intracellular Uptake of the Chol-Dox/TPGS Nanoassemblies Measured by Flow Cytometry: To evaluate intracellular uptake mechanism of the Chol-Dox/TPGS nanoassemblies in MCF-7 and MDA-MB-231 cell lines, first, cells were seeded into 48-well plates (1.5×10^5 cells/well), cultivated overnight in supplemented RPMI-1640 medium, and then incubated with the Chol-Dox/TPGS nanoassemblies (the absolute DOX concentration was set as 10 µg mL^{-1}) for 4 h, using the Chol-Dox as the control. The MCF-7 and MDA-MB-231 cells were then individually washed with 0.1 M PBS for three times. After trypsinization (EDTA-trypsin 0.25%), the process was followed by centrifugation at 2000 rpm for 8 min to harvest the cell pellets. Then, the harvested cell pellets were resuspended in 0.1 M PBS and put into 96-well plates, and then fluorescence intensity was measured using a flow cytometer (NovoCyte, ACEA Biosciences, Inc.). Here, MCF-7 and MDA-MB-231 cells (counts: 10 000 cells) were gated by sideward scatter versus forward scatter (SSC/FSC) plots, and fluorescence measurements were conducted in the PE channel (572 nm). Relative fluorescence intensity (cellular uptake efficiency) was normalized to that of cells with Chol-Dox as the indicator of 100% cellular uptake. In each case (Chol-Dox/TPGS nanoassemblies and the controls), the measurements were performed with three replicates ($n = 3$).

Endocytosis Assay of the Chol-Dox/TPGS Nanoassemblies with Various Endocytosis Inhibitors[39]: The cell lines were seeded in 24-well plates (5 × 10^5 cells/well) and incubated in culture medium (RPMI-1640 medium, with 10% FBS and 1% antibiotic-antimycotic solution) at 37 °C with 5% CO_2 for 24 h. The endocytosis-specific inhibitors (including: chlorpromazine (CPZ, clathrin-mediated endocytosis pathway inhibitor, 3.0 μg mL^{-1}), cytochalasin D (CYTO, macropinocytosis and phagocytosis pathway inhibitor, 2.3 μg mL^{-1}), nocodazole (NOCO, microtubule-assisted phagocytosis inhibitor, 2.0 μg mL^{-1}), filipin (FILI, lipid-raft pathway inhibitor, 10.0 μg mL^{-1}) and nigericin (NIGE, lysosome acidification inhibitor) were separately added into the MCF-7 and MDA-MB-231 cells and further incubated for 1 h.[39] Thereafter, the medium was replaced with fresh serum-free culture medium, and a predetermined volume of samples (Chol-Dox/TPGS assemblies, TPGS, Chol-Dox, and free Dox, 10 μg mL^{-1}, 70 μL) was added. Cells were further incubated at 37 °C for 4 h, then washed with 0.1 M PBS for three times and followed by trypsinization (EDTA-trypsin 0.25%). Afterward, centrifugation was done at 2000 rpm for 8 min to harvest the cell pellets. The harvested cell pellets were resuspended in 0.1 M PBS and put into 96-well plates, the fluorescence intensities were measured by flow cytometer (NovoCyte, ACEA Biosciences, Inc.). Here, MCF-7 and MDA-MB-231 cells (counts: 10 000 cells) were gated by SSC/FSC plots, and fluorescence measurements were conducted in the PE channel (572/28 nm). Relative fluorescence intensity (cellular uptake efficiency) was normalized to that of cells with Chol-Dox as the indicator of 100% cellular uptake. Each sample and control were measured with three replicates ($n = 3$).

Intracellular Localization of the Chol-Dox/TPGS Nanoassemblies: MCF-7 and MDA-MB-231 cell lines were seeded into 24-well microplates (5 × 10^5 cells/well in 1 mL RPMI-1640 medium with 10% FBS and 1% antibiotic-antimycotic solution) and incubated at 37 °C under 5% CO_2 for 24 h. Then the as-prepared Chol-Dox/TPGS nanoassemblies, TPGS, Chol-Dox, and free Dox solutions (Chol-Dox/TPGS assemblies, Chol-Dox, and free Dox were set as 10 μg mL^{-1} of Dox, 70 μL) were added into each well and incubated for 4 h. Thereafter, Hoechst 33258 (for cell nuclei staining, 50 μg per well) and Lysotracker (for lysosome staining, 150 μg per well) were added and incubated for 30 min to stain the cell nuclei and lysosome. Finally, the MCF-7 and MDA-MB-231 cells were washed with PBS for three times and the fluorescent images were recorded by fluorescence microscopy (Nikon Eclipse TE 2000E).

Supporting Information

Supporting Information is available from the Wiley Online Library or from the author.

Acknowledgements

The authors greatly acknowledge ARDITI-Agência Regional para o Desenvolvimento da Investigação Tecnologia e Inovação and Madeira 14-20 Program (project M1420-01-0145-FEDER- 000005-Centro de Química da Madeira-CQM$^+$), FCT-Fundação para a Ciência e a Tecnologia (Base Fund UIDB/00674/2020 and Programmatic Fund UIDP/00674/2020, Portuguese Government funds). A.R.N., M.V., and R.S. also acknowledge ARDITI for their fellowship grants ARDITI-CQM-2017-ISG-003, ARDITI-CQM- 2017-PDG-009 and ARDITI-CQM-2017-PDG-011, respectively.

Conflict of Interest

The authors declare no conflict of interest.

Author Contributions

F.O.: data curation, formal analysis, investigation, methodology, writing-review and editing. A.R.N.: data curation, formal analysis, funding acquisition, investigation, methodology, writing-review and editing. M.V.: data curation, formal analysis, funding acquisition, investigation, methodology, writing-review and editing. R.S.: conceptualization, funding acquisition, investigation, methodology, project administration, supervision, writing-original draft, writing-review and editing.

Keywords

cellular uptake, cholesterol, doxorubicin, endocytosis pathway, intracellular localization, prodrug, self-assembly

Received: November 1, 2020
Revised: February 28, 2021
Published online: April 6, 2021

[1] U. Kanwal, N. Irfan Bukhari, M. Ovais, N. Abass, K. Hussain, A. Raza, *J. Drug Targeting* **2018**, *26*, 296.
[2] S. V. Mussi, R. Sawant, F. Perche, M. C. Oliveira, R. B. Azevedo, L. A. Ferreira, V. P. Torchilin, *Pharm. Res.* **2014**, *31*, 1882.
[3] G. Chakravarty, A. Mathur, P. Mallade, S. Gerlach, J. Willis, A. Datta, S. Srivastav, A. B. Abdel-Mageed, D. Mondal, *Biochimie* **2016**, *124*, 53.
[4] M. Gonçalves, S. Mignani, J. Rodrigues, H. Tomás, *J. Controlled Release* **2020**, *317*, 347.
[5] J. L. Zaro, *AAPS J.* **2015**, *17*, 83.
[6] D. Irby, C. Du, F. Li, *Mol. Pharmaceutics* **2017**, *14*, 1325.
[7] A. Maksimenko, F. Dosio, J. Mougin, A. Ferrero, S. Wack, L. H. Reddy, A.-A. Weyn, E. Lepeltier, C. Bourgaux, B. Stella, L. Cattel, P. Couvreur, *Proc. Natl. Acad. Sci. USA* **2014**, *111*, E217.
[8] F. Li, C. Snow-Davis, C. Du, M. L. Bondarev, M. D. Saulsbury, S. O. Heyliger, *J. Visualized Exp.* **2016**, *114*, e54338.
[9] C. Liang, W. Ye, C. Zhu, R. Na, Y. Cheng, H. Cui, D.-Z. Liu, Z.-F. Yang, S.-Y. Zhou, *Mol. Pharmaceutics* **2014**, *11*, 1378.
[10] S. Zhao, L. V. Minh, N. Li, V. M. Garamus, U. A. Handge, J. Liu, R. Zhang, R. Willumeit-Römer, A. Zou, *Colloids Surf., B* **2016**, *145*, 95.
[11] M. A. Albrecht, C. W. Evans, C. L. Raston, *Green Chem.* **2006**, *8*, 417.
[12] L. Ge, W. Qi, L. Wang, H. Miao, Y. Qu, B. Li, B.-L. Song, *Proc. Natl. Acad. Sci. USA* **2011**, *108*, 551.
[13] Z. Ma, X. X. Zhu, *Mol. Pharmaceutics* **2018**, *15*, 2348.
[14] V. Janout, L. H. Zhang, I. V. Staina, C. Di Giorgio, S. L. Regen, *J. Am. Chem. Soc.* **2001**, *123*, 5401.
[15] A. J. Cunningham, M. Robinson, X. Banquy, *Mol. Pharmaceutics* **2018**, *15*, 1266.
[16] Z. Wang, T. Luo, R. Sheng, H. Li, J. Sun, A. Cao, *Biomacromolecules* **2016**, *17*, 98.
[17] Z. Wang, T. Luo, A. Cao, J. Sun, L. Jia, R. Sheng, *Nanomaterials* **2018**, *8*, 136.
[18] R. Sheng, T. Luo, Y. Zhu, H. Li, J. Sun, S. Chen, W. Sun, A. Cao, *Biomaterials* **2011**, *32*, 3507.
[19] R. Sheng, T. Luo, H. Li, J. Sun, Z. Wang, A. Cao, *Bioorg. Med. Chem.* **2013**, *21*, 6366.
[20] R. Sheng, T. Luo, H. Li, J. Sun, Z. Wang, A. Cao, *Colloids Surf., B* **2014**, *116*, 32.
[21] J. S. Suk, Q. Xu, N. Kim, J. Hanes, L. M. Ensign, *Adv. Drug Delivery Rev.* **2016**, *99*, 28.
[22] H. Hatakeyama, H. Akita, H. Harashima, *Adv. Drug Delivery Rev.* **2011**, *63*, 152.
[23] H. Maeda, *Adv. Drug Delivery Rev.* **2015**, *91*, 3.
[24] Z. Zhang, S. Tan, S. S. Feng, *Biomaterials* **2012**, *33*, 4889.
[25] M. R. Vijayakumar, M. S. Muthu, S. Singh, *Expert Opin. Drug Delivery* **2013**, *10*, 529.
[26] X. Meng, J. Liu, X. Yu, J. Li, X. Lu, T. Shen, *Sci. Rep.* **2017**, *7*, 2964.
[27] C. Yang, T. Wu, Y. Qi, Z. Zhang, *Theranostics* **2018**, *8*, 464.

[28] Y. Guo, J. Luo, S. Tan, B. O. Otieno, Z. Zhang, *Eur. J. Pharm. Sci.* **2013**, *49*, 175.
[29] S. Xiang, H. Tong, Q. Shi, J. C. Fernandes, T. Jin, K. Dai, X. Zhang, *J. Controlled Release* **2012**, *158*, 371.
[30] L. Ge, W. Qi, L. J. Wang, H. H. Miao, Y. X. Qu, B. L. Li, B.-L. Song, *Proc. Natl. Acad. Sci. USA* **2011**, *108*, 551.
[31] Y. U. Bae, B. K. Kim, J. W. Park, Y. B. Seu, K. O. Doh, *Mol. Pharmaceutics* **2012**, *9*, 3579.
[32] D. Pozzi, C. Marchini, F. Cardarelli, A. Rossetta, V. Colapicchioni, A. Amici, M. Montani, S. Motta, P. Brocca, L. Cantù, G. Caracciolo, *Mol. Pharmaceutics* **2013**, *10*, 4654.
[33] R. Sheng, Z. Wang, T. Luo, A. Cao, J. Sun, J. M. Kinsella, *Int. J. Mol. Sci.* **2018**, *19*, 369.
[34] S. Mignani, J. Rodrigues, H. Tomas, M. Zablocka, X. Shi, A.-M. Caminade, J.-P. Majoral, *Chem. Soc. Rev.* **2018**, *47*, 514.
[35] V. Estrella, T. Chen, M. Lloyd, J. Wojtkowiak, H. H. Cornnell, A. Ibrahim-Hashim, K. Bailey, Y. Balagurunathan, J. M. Rothberg, B. F. Sloane, J. Johnson, R. A. Gatenby, R. J. Gillies, *Cancer Res.* **2013**, *73*, 1524.
[36] R. Sheng, X. Zhuang, Z. Wang, A. Cao, K. Lin, J. Zhu, *Nanomaterials* **2016**, *6*, 69.
[37] Z. Wang, Z. Luo, M. Li, R. Sheng, T. Luo, A. Cao, *Acta Polym. Sin.* **2016**, *5*, 667.
[38] P. Sundaramoorthy, R. Baskaran, S. K. Mishra, K. Y. Jeong, S. H. Oh, B. Kyu Yoo, H. M. Kim, *Colloids Surf., B* **2015**, *135*, 793.
[39] H. Li, T. Luo, R. Sheng, J. Sun, Z. Wang, A. Cao, *Biomaterials* **2013**, *34*, 7923.
[40] J. Sun, R. Sheng, T. Luo, Z. Wang, H. Li, A. Cao, *J. Mater. Chem. B* **2016**, *4*, 4696.
[41] C. M. LaManna, H. Lusic, M. Camplo, T. J. McIntosh, P. Barthélémy, M. W. Grinstaff, *Acc. Chem. Res.* **2012**, *45*, 1026.
[42] Z. Wang, R. Sheng, T. Luo, J. Sun, A. Cao, *Polym. Chem.* **2017**, *8*, 472.
[43] S. K. Misra, S. Naz, P. Kondaiah, S. Bhattacharya, *Biomaterials* **2014**, *35*, 1334.
[44] S. Sarett, T. A. Werfel, I. Chandra, M. A. Jackson, T. E. Kavanaugh, M. E. Hattaway, T. D. Giorgio, C. L. Duvall, *Biomaterials* **2016**, *97*, 122.
[45] F. Sheikhi Mehrabadi, W. Fischer, R. Haag, *Curr. Opin. Solid State Mater. Sci.* **2012**, *16*, 310.
[46] Y. Zhang, C. Yang, W. Wang, J. Liu, Q. Liu, F. Huang, L. Chu, H. Gao, C. Li, D. Kong, Q. Liu, J. Liu, *Sci. Rep.* **2016**, *6*, 21225.
[47] Y. Shan, T. Luo, C. Peng, R. Sheng, A. Cao, X. Cao, M. Shen, R. Guo, H. Tomás, X. Shi, *Biomaterials* **2012**, *33*, 3025.
[48] A. F. Adler, K. W. Leong, *Nano Today* **2010**, *5*, 553.
[49] G. Sahay, D. Y. Alakhova, A. V. Kabanov, *J. Controlled Release* **2010**, *145*, 182.
[50] G. Scambia, S. Mancuso, P. B. Panici, R. De Vincenzo, G. Ferrandina, G. Bonanno, F. O. Ranelletti, M. Piantelli, A. Capelli, *Int. J. Cancer* **1993**, *54*, 462.
[51] S. F. Tehrani, F. Bernard-Patrzynski, I. Puscas, G. Leclair, P. Hildgen, V. G. Roullin, *Nanomedicine* **2019**, *16*, 185.
[52] A. G. Assanhou, W. Li, L. Zhang, L. Xue, L. Kong, H. Sun, R. Mo, C. Zhang, *Biomaterials* **2015**, *73*, 284.
[53] B. Shi, H. Zhang, Z. Shen, J. Bi, S. Dai, *Polym. Chem.* **2013**, *4*, 840.
[54] B. Tian, Y. Ding, J. Han, J. Zhang, Y. Han, J. Han, *Colloids Surf., B* **2015**, *130*, 246.
[55] C. P. Cerrato, K. Künnapuu, Ü. Langel, *Expert Opin. Drug Delivery* **2017**, *14*, 245.